Extreme Mechanics Letters 31 (2019) 100542

Contents lists available at ScienceDirect

Extreme Mechanics Letters

journal homepage: www.elsevier.com/locate/eml

How inhomogeneous zipping increases the force output of Peano-HASEL actuators

Philipp Rothemund [a], Nicholas Kellaris [a,b], Christoph Keplinger [a,b,*]

[a] Department of Mechanical Engineering, University of Colorado, Boulder, CO 80309, USA
[b] Materials Science and Engineering Program, University of Colorado, Boulder, CO 80303, USA

ARTICLE INFO

Article history:
Received 3 July 2019
Received in revised form 13 August 2019
Accepted 13 August 2019
Available online 16 August 2019

Keywords:
Soft robotics
Peano-HASEL actuator
Artificial muscle
Model
Instability

ABSTRACT

Research in soft robotics has yielded numerous types of soft actuators with widely differing mechanisms of operation that enable functionality that is difficult or impossible to reproduce with hard actuators such as electromagnetic motors. The Peano-HASEL (hydraulically amplified self-healing electrostatic) actuator is a new type of electrostatic, linearly contracting, soft actuator that features large strains, fast actuation, and high energy densities. Peano-HASEL actuators are comprised of pouches, which are made of flexible dielectric polymer films, filled with a liquid dielectric, and covered with flexible electrodes. When a voltage is applied to the electrodes, they "zip" together due to the Maxwell stress, which displaces the liquid inside the pouch, and causes the actuator to contract. Zipping can occur homogeneously or inhomogeneously. In this letter we analyze inhomogeneous zipping and its influence on the performance of Peano-HASEL actuators. We develop a theoretical model that describes inhomogeneous as well as homogeneous zipping of the electrodes and characterize the behavior of actuators experimentally. Inhomogeneous zipping occurs (depending on the size of the electrodes) predominantly at large loads, because it allows for larger areas of the electrodes to be zipped. Inhomogeneous zipping increases the blocking force of the actuators and leads to larger actuation strains near the blocking force. Exploiting inhomogeneous zipping by increasing the electrode size enables an increase in the blocking force of the actuators by up to 47%.

1. Introduction

Soft actuators have enabled the design of robots that allow safe human–machine interaction, require less control, and perform better in unstructured environments than robots consisting only of hard components [1–6]. A variety of soft actuator technologies has been developed that use widely differing physical principles to function. In fluidic soft actuators – the most prominent of these technologies – gaseous or liquid fluids pressurize or depressurize deformable channels [3,7,8]. Another prevalent mechanism for soft actuation is the use of electrostatic fields, such as in dielectric elastomer actuators (DEAs), which consist of thin elastomeric membranes that deform due to the Maxwell stress resulting from an electric field across their thickness [9–11]. Other mechanisms use temperature- [12–14], electric-field- [15] or pH-induced [16] volume changes, magnetic fields [17], or optical stimuli [18] to induce deformation. HASEL (hydraulically amplified self-healing electrostatic) actuators combine the advantages of dielectric elastomer actuators and fluidic actuators, as they use an electric-field-induced Maxwell stress to deform soft, fluid-filled structures [19,20]. HASEL actuators stand out among other soft actuators for their versatility [21] and high performance, with linear actuation strains larger than 100%, actuation frequencies larger 100 Hz, and theoretical energy densities larger than 10,000 J/kg [19–22].

One design of a HASEL actuator – the Peano-HASEL actuator [20] – exhibits linear contraction on activation, which makes it particularly interesting for robotics applications. These actuators consist of a rectangular liquid-filled pouch that is covered on both sides with deformable electrodes (Fig. 1a). The shell of the pouch is formed by bonding two flexible (but not stretchable) films. The shell is filled with a liquid dielectric. Forces can be applied to the actuator through rigid frames attached to the top and the bottom of the pouch. When a voltage is applied between the electrodes, the resulting electric field causes the electrodes to zip together from the top [20,23], which displaces the liquid dielectric inside the pouch (Fig. 1b). Because the shell is inextensible, the actuator contracts (Δx).

For Peano-HASEL actuators with rectangular electrodes that cover half or less of the pouch length (such as the one shown in Fig. 1c), the electrode zipping progresses at small loads approximately homogeneously from the top of the pouch (Fig. 1d, Movie

* Corresponding author at: Department of Mechanical Engineering, University of Colorado, Boulder, CO 80309, USA.
E-mail address: Christoph.Keplinger@colorado.edu (C. Keplinger).

https://doi.org/10.1016/j.eml.2019.100542
2352-4316/

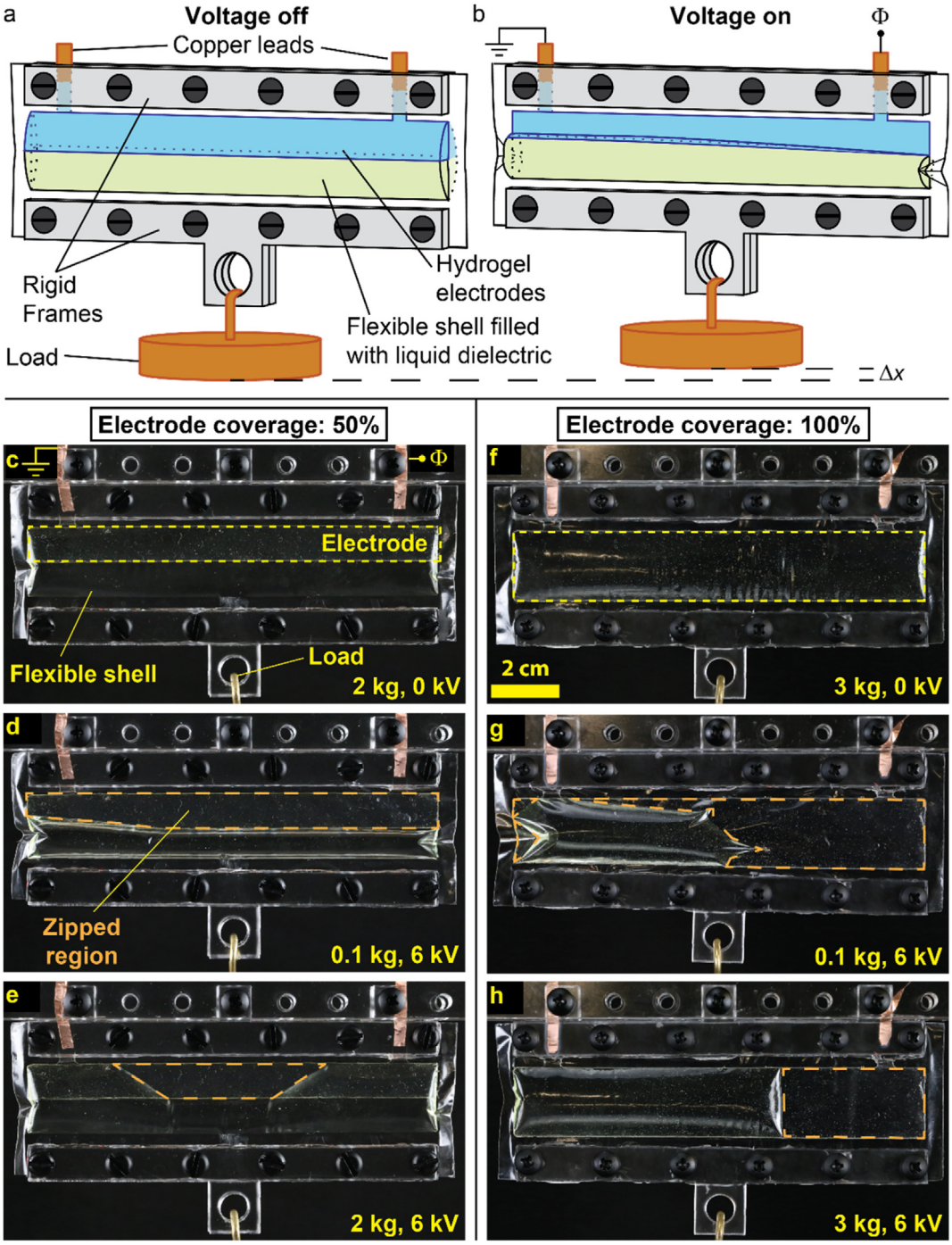

Fig. 1. Electrostatic zipping in Peano-HASEL actuators. (a) Schematic of the structure of a Peano-HASEL actuator. (b) When a voltage is applied to the electrodes, they zip together from the top of the liquid-filled shell and the actuator contracts in length. (c) Photograph of a Peano-HASEL actuator with electrodes that cover half of the length of the shell under a mechanical load of 2 kg. (d) At a small load of 0.1 kg, when a voltage of 6 kV is applied to the actuator, the actuator zips from the top across the entire width. (e) At a large load of 2 kg the electrodes zip only in the center. (f) Photograph of a Peano-HASEL actuator with electrodes that cover the entire liquid-filled shell under a mechanical load of 3 kg. (g) When a voltage of 6 kV is applied to the electrodes at a small load of 0.1 kg, the actuator zips irregularly. (h) At a large load of 3 kg the electrodes zip from the side.

S1). For this mode of actuation, we previously developed an analytical model to describe the quasi-static actuation behavior [22]. At large loads that are close to the blocking force (the maximum force the actuator can generate), however, these Peano-HASEL actuators form multiple regions in which the electrodes are either completely zipped or unzipped (Fig. 1e, Movie S1). In that force range, the experimentally observed actuation strains exceeds the model predictions [22]. Peano-HASEL actuators with rectangular electrodes that cover more than half of the pouch length (such as when the entire shell is covered by the electrodes, Fig. 1f) typically do not zip homogeneously (Fig. 1g, h, Movie S2).

In this letter we analyze inhomogeneous zipping and its influence on the performance of Peano-HASEL actuators. We derive an electromechanical model that includes inhomogeneous zipping for the quasi-static behavior of these actuators with a focus on understanding the behavior close to the blocking force. We find that inhomogeneous zipping occurs as it is energetically favorable compared to homogeneous zipping; further, because

inhomogeneous zipping allows larger areas of electrode to be zipped at a given strain, the actuator produces higher forces when the electrodes zip inhomogeneously. We validate the model experimentally and demonstrate its accuracy in predicting the force–strain behavior at high forces up to the blocking force. These results can be leveraged to design actuators with increased force output at low strains.

2. Model for inhomogeneous zipping

The model we derive in this section is intended to describe the behavior of Peano-HASEL actuators at large loads close to the blocking force, when it splits into distinct regions with different states of zipping (Fig. 1e, h). Limiting the validity of the model to this range of loads allows us to describe the shape of the zipped actuator with a finite number (five) of degrees of freedom and to determine the equilibrium state by minimizing the total free energy of the system (energy of the actuator, the voltage source, and the mechanical load). This model is based on previous models for Peano-HASEL actuators for homogeneous zipping [22,24]. We choose a similar parametrization for the geometry and neglect the influence of elasticity, the electric field inside the fluid-filled region of the pouch, and boundary effects on the shape of the actuator. Using the model, we analyze the free energy of the system to investigate the mechanism for inhomogeneous zipping and compare the calculated force–strain behavior of inhomogeneous zipping and homogeneous zipping.

2.1. Parametrization of the geometry

The shell of the pouch consists of two rectangular films of thickness t bonded together at the edges, so that the sheets form a rectangular pouch of width w, and length L (Fig. 2a). The pouch is filled with an incompressible liquid dielectric of volume V_0. The top part of the shell is covered on both sides with electrodes of width w, and length L_E. The top edge of the actuator is clamped, and a tensile force F is applied to the bottom edge through a rigid bar. We assume that the films are inextensible and thin so that their bending stiffness can be neglected [22]. We also neglect boundary effects at the ends of the pouch. With these assumptions, the hydrostatic pressure inside the pouch deforms the shell into the shape of cylinder sections with intersection angle $2\alpha_0$ (Fig. 2a) [22,24,25]. The value of α_0 can be calculated from

$$V_0 = L^2 w \frac{2\alpha_0 - \sin(2\alpha_0)}{4\alpha_0^2} \tag{1}$$

and the initial length l_0 of the actuator from

$$l_0 = L \frac{\sin(\alpha_0)}{\alpha_0}. \tag{2}$$

When a voltage Φ is applied to the electrodes, an electric field arises between them, which causes an attractive Maxwell stress [10]. When this Maxwell stress becomes large enough, the electrodes begin to zip together from the top of the actuator, where the distance between the electrodes is the smallest and the Maxwell stress therefore the largest. Here we focus on large forces at which the actuator splits into separate regions of homogeneous zipping (Fig. 1e, h). In addition to neglecting boundary effects at the ends of the pouch and the bending stiffness of the film that forms the shell, we make the following simplifying assumptions: (i) we neglect the narrow transition zone between differently zipped regions and assume that the transition between differently zipped regions occurs in a discrete step; (ii) we neglect rotation of the bottom edge of the actuator relative to the top edge (this assumption is good at large loads, as the experimentally observed rotations are small).

These simplifications allow us to model the actuator with two parallel, coexistent states [26–31] of different homogeneous zipping lengths (Fig. 2b). The two regions can be parameterized with the zipping lengths z_1 and z_2, and the intersection angles $2\alpha_1$ and $2\alpha_2$. The widths of the regions are described by the variable x ($0 \le x \le 1$). Experimentally, we also observed cases in which the actuator splits into three coexistent regions of states of zipping (*e.g.*, Fig. 1e). At large forces, two of these regions showed the same state of zipping. In the model, the two regions of equal zipping can be combined to a single zone, because it leads to the same free energy, so that this case is also described by Fig. 2b.

Because of the incompressibility of the liquid dielectric, the volume of the pouch does not change during actuation:

$$\begin{aligned} V_0 = {} & xw\,(L - z_1)^2 \frac{2\alpha_1 - \sin(2\alpha_1)}{4\alpha_1^2} \\ & + (1-x)\,w\,(L - z_2)^2 \frac{2\alpha_2 - \sin(2\alpha_2)}{4\alpha_2^2}. \end{aligned} \tag{3}$$

The first term on the right-hand side of Eq. (3) describes the volume of the liquid filled portion of the pouch of region 1, and the second term that of region 2. Because rotation of the bottom edge of the actuator is neglected, both regions have the same length l which can be calculated as

$$l = z_1 + (L - z_1)\frac{\sin(\alpha_1)}{\alpha_1} = z_2 + (L - z_2)\frac{\sin(\alpha_2)}{\alpha_2}. \tag{4}$$

We define the actuation strain as

$$e = 1 - \frac{l}{l_0}. \tag{5}$$

Homogeneous zipping (Fig. 2c) is a special case of inhomogeneous zipping, in which either $\alpha_1 = \alpha_2 = \alpha_h$, and $z_1 = z_2 = z_h$ (in this case x is undefined), $x = 0$ (α_1 and z_1 are undefined), or $x = 1$ (α_2 and z_2 are undefined) .

2.2. Free energy of the system

The total free energy H of the system is comprised of the free energies of the actuator, the voltage source, and the mechanical load. Because we neglect the bending stiffness of the film that forms the shell and treat it as inextensible, the only contribution of the actuator to H is the electrical energy stored in the electric field between the electrodes. We only consider the electrical energy stored in the zipped regions of the electrodes because the magnitude of the electric field decays rapidly in the unzipped region [22,24]. Assuming that there is no oil between the zipped films, the zipped region can be treated as a parallel plate capacitor with capacitance

$$C = \frac{\varepsilon w\,[x z_1 + (1-x)\,z_2]}{2t}, \tag{6}$$

where ε is the permittivity of the shell. When charges Q are deposited on the electrodes, the free energy of the actuator therefore becomes

$$H_a = \frac{1}{2}\frac{Q^2}{C}. \tag{7}$$

When charges flow from the voltage source to the actuator, the free energy of the voltage source decreases by $-Q\Phi$, and when the actuator deforms the free energy of the load changes by $-F(l - l_0)$. The total free energy of the system can therefore be calculated as

$$H = \frac{1}{2}\frac{Q^2}{C} - Q\Phi - F(l - l_0). \tag{8}$$

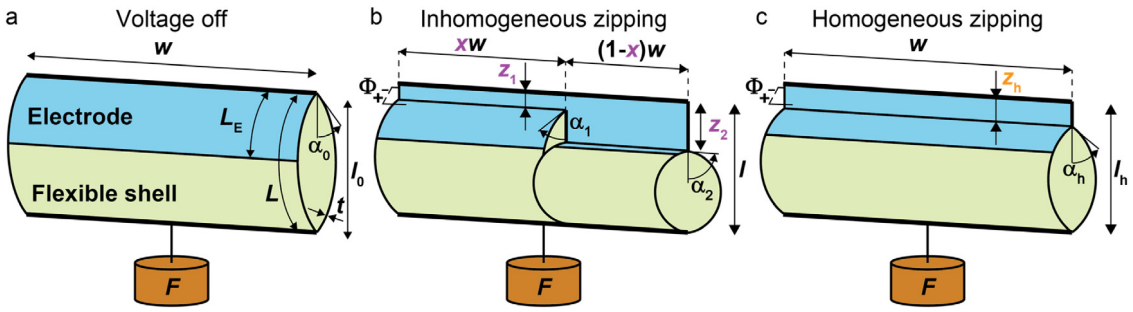

Fig. 2. Homogeneous and inhomogeneous zipping in Peano-HASEL actuators. (a) Parametrization of the geometry of the Peano-HASEL actuator under a mechanical load F. The shell of the pouch consists of two flexible films of width w, length L, and thickness t. When filled with a liquid dielectric, the films form two cylinder sections with intersection angle $2\alpha_0$ so that the length of the actuator becomes l_0. The top of the pouch is covered on both sides with electrodes of width w and length L_E. (b) Parametrization of the geometry for inhomogeneous zipping. When a voltage Φ is applied to the electrodes, they zip together from the top and form two distinct regions of different zipping lengths (z_1, z_2), intersection angles ($2\alpha_1$, $2\alpha_2$), and widths ($xw, (1-x)w$). Overall, the actuator contracts to a length l. (c) Homogeneous zipping is a special case of actuation, in which both regions zip equally (*i.e.*, $z_1 = z_2 = z_h$, $\alpha_1 = \alpha_2 = \alpha_h$), or one of the regions has zero width ($x = 1$ or $x = 0$). The actuator contracts to a length l_h.

2.3. Minimization of free energy

In this section we describe how to minimize H in order to obtain the equilibrium states of the actuator. Minimization of Eq. (8) with respect to Q leads to the well-known relationship between capacitance, voltage, and charge: $Q = C\Phi$. Using this relationship, we rewrite Eq. (8) to

$$H = -\frac{1}{2}C\Phi^2 - F(l - l_0). \tag{9}$$

The first term on the right-hand side of Eq. (9) describes the total electrical energy of the system. The second term describes the mechanical energy of the load. To elucidate the influence of the degrees of freedom and the applied load and voltage on these terms we rewrite Eq. (9) in a dimensionless form by substituting Eqs. (4) and (6) into Eq (9):

$$\begin{aligned}\frac{Ht}{wL_E\varepsilon\Phi^2} = &-\frac{1}{4}\left(x\frac{z_1}{L_E} + (1-x)\frac{z_2}{L_E}\right)\\ &- \frac{Ft}{w\varepsilon\Phi^2}\left(\frac{z_1}{L_E} + \left(\frac{1}{f_E} - \frac{z_1}{L_E}\right)\frac{\sin(\alpha_1)}{\alpha_1} - \frac{l_0}{L_E}\right),\end{aligned} \tag{10}$$

where the electrode coverage $f_E = L_E/L$ describes the fraction of the pouch length that is covered by electrodes.

Eq. (10) shows that for a given geometry and fill volume of liquid dielectric, the equilibrium state of the actuator only depends only a single nondimensional load $Ft\ /\ (w\Phi^2\varepsilon)$, which combines the mechanical load and the applied voltage. By way of example we assume for the further discussion that the length of the electrodes is $L_E = 0.5\ L$ (i.e., $f_E = 0.5$) and that the volume of the liquid dielectric inside the actuator is $V = L^2w\ /\ 4\pi$. In this case, the liquid-filled region of the pouch has the shape of a cylinder when the electrodes are completely zipped [22].

Eqs. (3) and (4) impose constraints that can be used to eliminate α_1 and α_2 as independent variables. The free energy then only depends on the degrees of freedom z_1, z_2, and x. For a constant x, the contours of the total free energy H can be plotted on the z_1-z_2 plane. Fig. 3a shows such a contour plot for the nondimensional load $Ft\ /\ (w\Phi^2\varepsilon) = 2$ at $x = 0.5$. The diagonal $z_1 = z_2$ corresponds to the special case of homogeneous zipping. On the diagonal, there is a saddle-point (indicated by an orange dot in Fig. 3a), which is the equilibrium state for homogeneous zipping. However, because H decreases in directions perpendicular to the diagonal $z_1 = z_2$ away from the saddle-point, states of lower energy exist, in which the electrodes zip inhomogeneously. There are two equal minima at the edges of the z_1-z_2 plane (indicated by purple dots in Fig. 3a). These minima would be the equilibrium states of the actuator if the partition of the actuator is fixed to $x = 0.5$.

Because x can vary and is, thus, not a priori known, the energy contours of H must be investigated as a function of x. The locations and the values of the off-diagonal minima on the z_1-z_2 plane change with x (Fig. 3b shows the energy contours for a value $x = 0.25$). The saddle-point on the diagonal does not, because x does not influence the shape of the actuator when the actuators zips homogeneously. Fig. 3c shows the values of the free energy of the absolute minima (H_i) and the saddle-point (H_h) as a function of x for the nondimensional load $Ft/(w\Phi^2\varepsilon) = 2$ (because of symmetry only values for $x \leq 0.5$ are shown). For inhomogeneous zipping, the absolute minimum with the overall smallest value of H_i occurs at $x = 0.41$. Because it is smaller than H_h, inhomogeneous zipping is energetically favorable to homogeneous zipping at this load. Fig. 3d shows that at $x = 0.41$, the absolute minimum on the $z_1 - z_2$ plane is located at $z_1 = 0$, and $z_2 = 1$. In equilibrium, one region of the electrodes is therefore completely zipped, and the other region completely unzipped. Changing the nondimensional load to $Ft/(w\Phi^2\varepsilon) = 7$ changes the partition of the actuator in equilibrium ($x = 0.16$, Fig. 3e), but one region remains completely zipped and the other completely unzipped ($z_1 = 1$, and $z_2 = 0$, Fig. 3f).

2.4. Equilibrium states

To calculate all equilibrium states of the actuator for inhomogeneous zipping from the blocking load to the free strain, we minimized equation Eq. (10) with the function *fmincon* in Matlab R2017 with respect to z_1, z_2, α_1, α_2, and x while varying the nondimensional load $Ft/(w\Phi^2\varepsilon)$. We used Eqs. (3) and (4) as nonlinear constraints and limited the variable space to $0 < z_1$, $z_2 < L_E$ (the electrode length limits zipping), $0 < \alpha_1$, $\alpha_2 < \pi/2$ (at the maximum angle, the shell forms a cylinder), and $0 \leq x \leq 1$ (at the extremes, the actuator consists only of one homogeneously zipped region). To determine the equilibrium states for homogeneous zipping, we followed the same procedure using the additional constraint $z_1 = z_2$.

In the case of homogeneous zipping, the model predicts that at $Ft\ /\ (w\Phi^2\varepsilon) = 0$, the electrodes of the actuator are completely zipped (Fig. 4a). When a load is applied to the actuator, the electrodes gradually unzip (z_h decreases) with increasing load until they are completely open at the blocking load (Fig. 4a). For inhomogeneous zipping, the model predicts that the actuator split at all loads into two regions: one region is completely zipped, the other completely unzipped (Fig. 4a). At $Ft\ /\ (w\Phi^2\varepsilon) = 0$ the width of the unzipped region is zero ($x = 0$), so that the

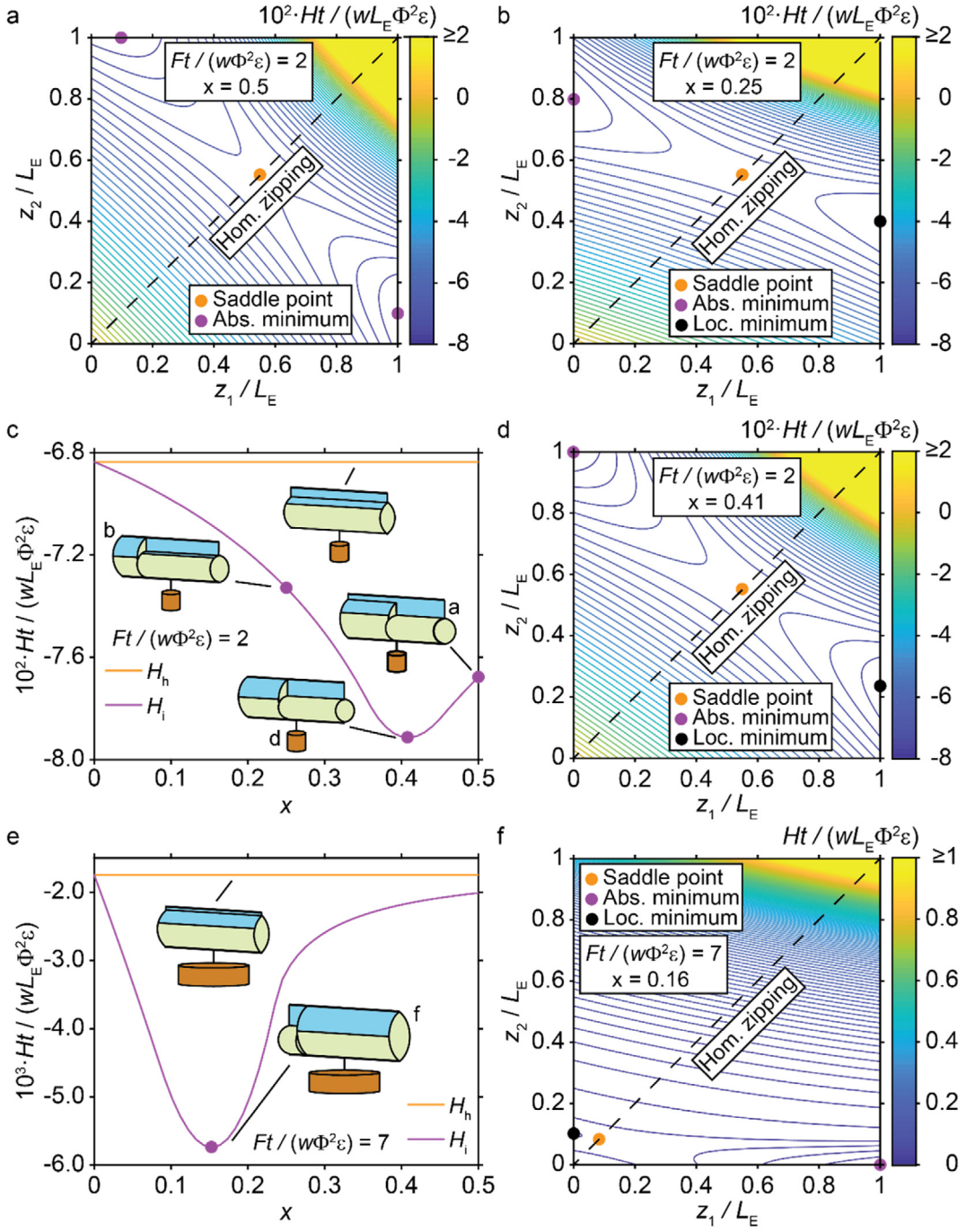

Fig. 3. Analysis of the free energy for homogeneous and inhomogeneous zipping. (a) Contours of the free energy as a function of z_1 and z_2 at the load $Ft / (w\Phi^2\varepsilon) = 2$ and $x = 0.5$. The equilibrium of homogeneous zipping (orange dot) is an unstable saddle point. At the minimum of the free energy, the actuator is zipped inhomogeneously (purple dots). (b) Contours of the free energy as a function of z_1 and z_2 at the load $Ft / (w\Phi^2\varepsilon) = 2$ and $x = 0.25$. A local (black dot) and a global (purple dot) minimum occurs. (c) Values of the absolute minima (H_i) and the saddle points (H_h) of the energy contours as a function of x at $Ft / (w\Phi^2\varepsilon) = 2$. Because of symmetry only the range $0 \leq x \leq 0.5$ is shown. (d) Contours of the free energy as a function of z_1 and z_2 at load $Ft / (w\Phi^2\varepsilon) = 2$ and $x = 0.41$. The absolute minimum of the free energy on this plane (purple dot) is the equilibrium for inhomogeneous zipping. (e) Values of the absolute minima and the saddle point of the energy contours as a function of x at $Ft / (w\Phi^2\varepsilon) = 7$. (f) Contours of the free energy as a function of z_1 and z_2 at load $Ft / (w\Phi^2\varepsilon) = 7$ and $x = 0.16$. The absolute minimum of the free energy on this plane (purple dot) is the equilibrium for inhomogeneous zipping. (a)–(f) The actuator has an electrode coverage $f_E = 0.5$ and fill $V = L^2 w / (4\pi)$. (For interpretation of the references to color in this figure, the reader is referred to the web version of this article.).

electrodes are completely zipped (Fig. 4b). When a load is applied to the actuator, x increases with the load until it reaches $x = 1$ at the blocking load (*i.e.*, the electrodes unzip sideways until they are completely unzipped) (Fig. 4b).

The free energy for inhomogeneous zipping is always smaller than the free energy of homogeneous zipping (Fig. S1), which implies that it is always energetically favorable compared to homogeneous zipping. Experimentally we observed that behavior only at large loads (Fig. 1e). At small loads the zipping behavior resembles that of homogeneous zipping (Fig. 1d). The likely reason is that we neglected the transition zone between the differently zipped regions in the model. The associated elastic energy prevents asymmetric zipping at small loads.

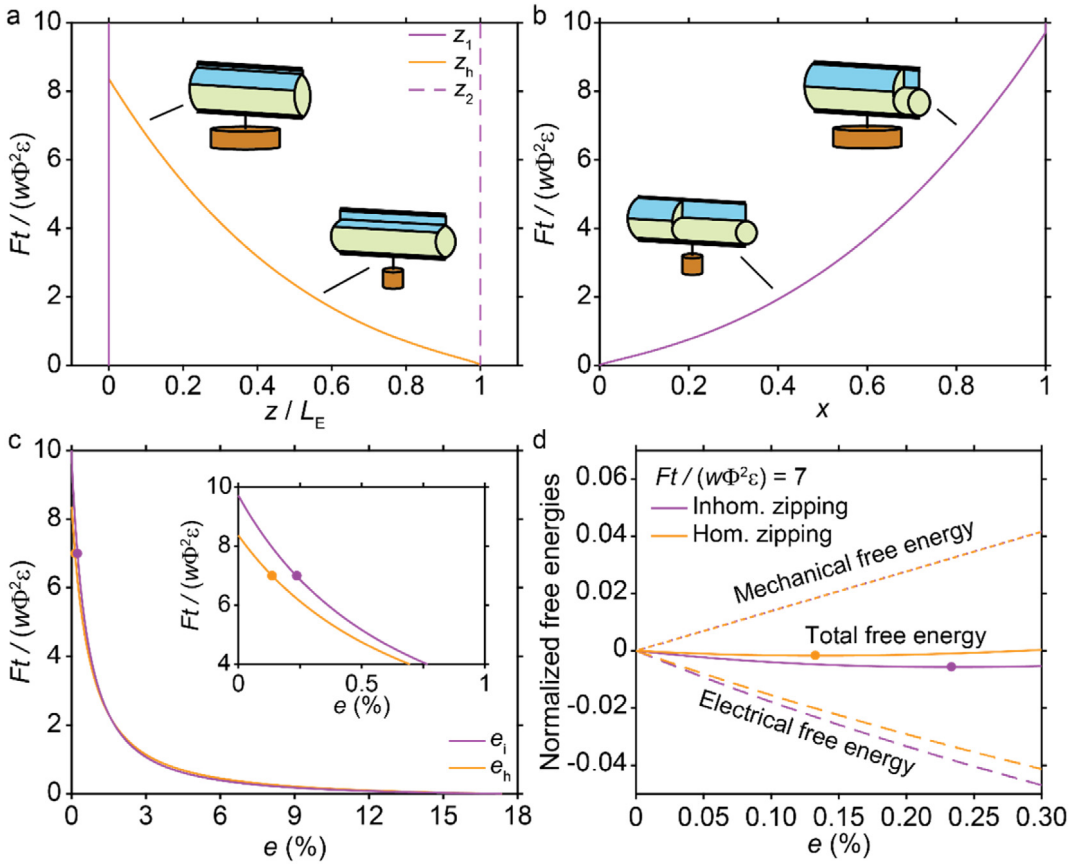

Fig. 4. Equilibrium states for inhomogeneous and homogeneous zipping. (a) For forces below the blocking force, the model predicts for homogeneous zipping that z_h increases when the load decreases (*i.e.*, the actuator zips from the top). For inhomogeneous zipping the model predicts for all loads that one region is completely unzipped (z_1) and one region is completely zipped (z_2). (b) When the actuator zips inhomogeneously, the model predicts that the value of x increases continuously with the load (*i.e.*, the actuator zips from the side). (c) Calculated force–strain curves for homogeneous (e_h) and inhomogeneous (e_i) zipping. Inhomogeneous actuation leads to larger strains at forces near the blocking force and an increased blocking force (inset). The dots mark the equilibria for inhomogeneous and homogeneous zipping at $Ft / (w\Phi^2\varepsilon) = 7$; (d) at $Ft / (w\Phi^2\varepsilon) = 7$, inhomogeneous zipping leads to a larger decrease in electrical free energy at a given strain, because a larger area of the electrodes zips. The mechanical energy of the load is identical for both cases. Thus, the minimum of the free energy for inhomogeneous zipping lies at a larger strain and a lower energy (purple dot). (a)–(d) The actuator has an electrode coverage $f_E = 0.5$ and fill $V = L^2 w / (4\pi)$. (For interpretation of the references to color in this figure, the reader is referred to the web version of this article.).

For both type of zipping the predicted free strain (the strain at $Ft / (w\Phi^2\varepsilon) = 0$) is 17% and the overall shape of the load–strain curve is very similar (Fig. 4c). The force–strain curve for homogeneous zipping calculated with the model introduced in this paper is identical to that predicted by the analytical model that we derived previously [22]. For inhomogeneous zipping, the model predicts, however, larger strains at large loads and a blocking load that is 16% larger than that of homogeneous zipping. This prediction is consistent with the behavior that we observed previously when comparing experimental data with the model for homogeneous zipping [22]. The increase in strain at large loads can be explained by analyzing the free energy of the actuator (Eq. (10)) at small strains. Due to the nonlinear relationship between the actuation strain and the area of zipped electrodes, inhomogeneous zipping leads, at the same strain, to a larger zipped area compared to homogeneous zipping (Fig. S1). Consequently, for inhomogeneous zipping the total electrical energy of the system (first term on the right-hand side of Eq. (10)) decreases faster than for homogeneous zipping (Fig. 4d). Because the increase in mechanical energy of the load with strain is the same for both types of zipping (second term on the right-hand side of Eq. (10)) (Fig. 4d), the minimum of the total free energy of the system lies at larger strains for inhomogeneous zipping (purple and orange dots in Fig. 4c, d).

3. Experimental validation and analysis

In this section we measure the force–strain curves for actuators with different electrode coverage f_E to validate the model. We also measure the blocking force and free strain of the actuators as a function of the electrode coverage and compare the experimental results with model predictions.

3.1. Experimental details

In all experiments we used actuators with pouches of 12 cm width and 2 cm length. We formed the shells by bonding two films of 18 μm-thick BOPP (Multi-Plastics, Inc; type 5020, relative dielectric permittivity $\varepsilon_r = 2.2$) with a CNC heat-sealer at a temperature of 195 ° C and 500 mm/min sealing speed [21]. Each pouch was filled with 3.8 ml Envirotemp FR3 (Cargill) as the liquid dielectric (at this volume, the liquid-filled region of the pouch of an actuator with electrode coverage $f_E = 0.5$ theoretically forms a cylinder when the electrodes are completely is zipped together). As electrodes we used polyacrylamide hydrogels swollen with an aqueous solution of LiCl [32,33] cut into shape with a laser cutter (Trotec Speedy360 Flexx). All electrodes had the same width as the pouch (12 cm) and lengths between 0.25 cm and 2.0 cm. We used conductive copper tape as leads to connect the electrodes to the voltage source and ground. We

attached acrylic bars of the same width as the pouch to the top and the bottom of the actuator for mounting and introduction of load.

We measured the deformation of the actuators under constant load using a 0.3 Hz square wave signal with 6 kV amplitude and reversing polarity (Trek Model 50/12 high voltage amplifier) to mitigate charge buildup in the shell [20]. As loads we used brass weights. We measured the actuation strain by optically tracking (Canon EOS 6D DSLR camera) a marker in the center of the acrylic bar at the bottom of the actuators.

3.2. Force–strain curves

We measured the force–strain curve of an actuator with electrode coverage $f_E = 0.5$ as a function of the load from the free strain to the blocking force (Fig. 5a). At small forces, the actuator zipped approximately homogeneously (Fig. 1d, Movie S1). With increasing load, the zipping of the electrodes became increasingly inhomogeneous until it reached (at $F \sim 20$ N) the extreme state of inhomogeneous zipping, in which one region of the electrodes was fully zipped and the remaining electrode region completely unzipped, as predicted by the model. For larger loads, the width of the zipped region of the electrodes decreased with increasing load as predicted by the model (Movie S1). The free strain of the actuator was $e_f = 12.5\%$ (Fig. 5a). With increasing load, the actuation strain decreased until it reached the blocking force $F_b = 44$ N.

The predictions of the model for homogeneous and inhomogeneous zipping both agree well with the experimental data. However, at large loads, the calculated strains for inhomogeneous zipping agree better with the experimental data (Fig. 5a, inset). Whereas the homogeneous model underestimates the blocking force by 11%, the predicted blocking force for inhomogeneous zipping lies within 3% of the experimentally measured blocking force.

Fig. 5b shows the force–strain curve of an actuator with $f_E = 1.0$. Even at low loads the actuator zipped irregularly (Fig. 1g, Movie S2), but only for $F \gtrsim 9$ N did the electrodes zip in cleanly separated regions as described by the model. The irregular zipping led to a large rotation of the bottom of the actuator at small loads (Fig. 1g), which reduced the free strain of the actuator to $e_f = 6.7\%$. The blocking force of the actuator increased to $F_b = 54$ N (Fig. 5b).

For homogeneous zipping of the actuator with $f_E = 1.0$, the model predicts the same force–strain curve as for $f_E = 0.5$, because the actuator cannot zip beyond the center of pouch due to geometric blocking [22]. Increasing the electrode coverage to $f_E > 0.5$ therefore has no influence on the force–strain curve for homogeneous zipping. The calculated force–strain curve for inhomogeneous zipping agrees well with the experimental data over a large range of forces (Fig. 5b, inset). The model for inhomogeneous zipping overestimates the blocking force by less than 7%. Like in the experiment, the model predicts for inhomogeneous zipping a decrease in free strain, so that the overall force–strain curve agrees better with the data. However, the better agreement in the range of small forces is coincidental, as the model neglects rotation of the bottom part of the actuator.

3.3. Blocking force and free strain as function of electrode coverage

At the blocking force, the model allows the electrodes to zip by a (theoretically infinitesimal) small amount. In the case of homogeneous zipping, the actuator zips from the top, so that the width of the initially zipped region (w) is independent of f_E and, consequently, also the predicted blocking force (orange line in Fig. 6a). For inhomogeneous zipping, the electrodes zip from the side, so that the width of this infinitesimal region is equal to the length of the electrodes ($L_E = f_E L$). In that case, the blocking force therefore depends on f_E (purple line in Fig. 6a). For $f_E \to 0$, the predicted blocking force for homogeneous and inhomogeneous zipping are equal ($F_b = 39$ N). For inhomogeneous zipping the model predicts an increase of F_b with f_E of up to 47% at $f_E = 1$. To validate this prediction, we measured the blocking force of actuators with electrode coverage $0.125 \leq f_E \leq 1.0$. In this range of f_E, the blocking force increased from $F_b = 40$ N at $f_E = 0.125$ to $F_b = 54$ N at $f_E = 1.0$ (Fig. 6a). The measured data agrees very well with the predicted values for inhomogeneous zipping.

Fig. 6b shows the free strain of the actuators as a function of f_E. For $f_E \leq 0.5$, the minimum energy state occurs when the electrodes are fully zipped. The free strain therefore increases with f_E. At the used volume of liquid dielectric ($V = L^2 w / 4\pi$), the liquid-filled region of the pouch of an actuator with $f_E = 0.5$ (in theory) forms the shape of a cylinder when the electrodes are completely zipped. In the case of homogeneous zipping, further deformation is therefore geometrically blocked for values $f_E > 0.5$ [22]. Experimentally, we observed for $f_E > 0.5$ that the electrodes zipped inhomogeneously when no load was applied, which lead to a rotation of the bottom of the actuators and thus to a reduction in free strain. The model predicts for inhomogeneous zipping a decrease in free strain, but because the assumptions of the model (assuming no rotation) are violated, the model should not be used to predict the free strain for $f_E > 0.5$.

4. Conclusions

In this letter we studied the zipping behavior of Peano-HASEL actuators theoretically and experimentally. We developed an electromechanical model that describes homogeneous and inhomogeneous zipping at large loads. With the help of the model we showed that inhomogeneous zipping occurs because it allows – at the same strain – larger areas of the electrodes to be zipped, reducing the total energy of the system compared to homogeneous zipping. This behavior leads to larger strains at forces close to the blocking force and increases the blocking force. When the entire pouch is covered with electrodes, inhomogeneous zipping increases the blocking force by ~47% compared to homogeneous zipping.

The derived model agrees well with the experimental data at large forces. Because of the simplifications that we made during the derivation it predicts that inhomogeneous deformation is always energetically favorable to homogeneous zipping, even at small loads. In order to obtain a more realistic prediction of the zipping behavior, the model would need to be extended by including rotation of the bottom edge of the actuator and elastic energy terms for the side constraints and the transition zone between the differently zipped regions. In the experiments, the actuators gradually transitioned from homogeneous to inhomogeneous zipping. From this observation we conclude that imperfections in the actuator such as wrinkles in the shell, material imperfections, or unequal load introduction nucleate the transition from homogeneous to inhomogeneous zipping [31]. The modeling of those defects may therefore have to be included to correctly describe the transition from homogeneous to inhomogeneous zipping. Additionally, we neglected dynamic effects which can influence the zipping behavior [22].

Even though we analyzed in this work only Peano-HASEL actuators, the underlying phenomenon can also lead to inhomogeneous zipping in other geometries of HASEL actuators and increase their actuation strains at forces close to the blocking force. The work also shows that without changing the geometry of the pouch of a Peano-HASEL actuator, its force characteristics can be modified by varying the electrode geometry. Exploiting inhomogeneous zipping in actuators with large electrodes allows the design of actuators with increased force output.

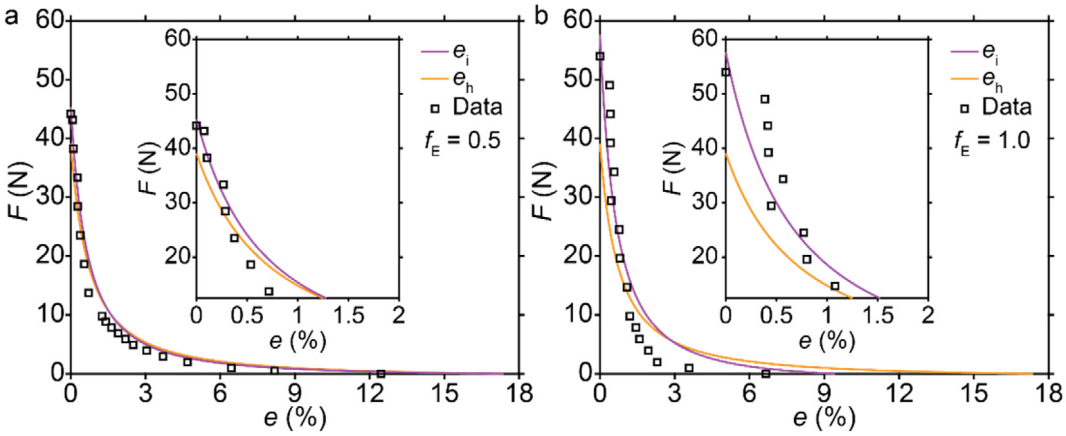

Fig. 5. Experimental validation of the modeling results. (a) Comparison of the measured force–strain curve to model predictions for homogeneous (e_h) and inhomogeneous (e_i) zipping for an actuator with electrode coverage $f_E = 0.5$. The inset shows that close to the blocking force, the modeling results for inhomogeneous zipping agree better with the data. (b) Comparison of the measured force–strain curve to the model predictions for homogeneous and inhomogeneous zipping for an actuator with electrode coverage $f_E = 1.0$. The inset shows the range of forces in which the model predictions for inhomogeneous zipping agree better with the data than the prediction for homogeneous zipping. The blocking force increased by 23% compared to the actuator with $f_E = 0.5$. (a)–(b) Both actuators have the fill volume $V = 3.8$ ml. The experiments were performed at $\Phi = 6$ kV.

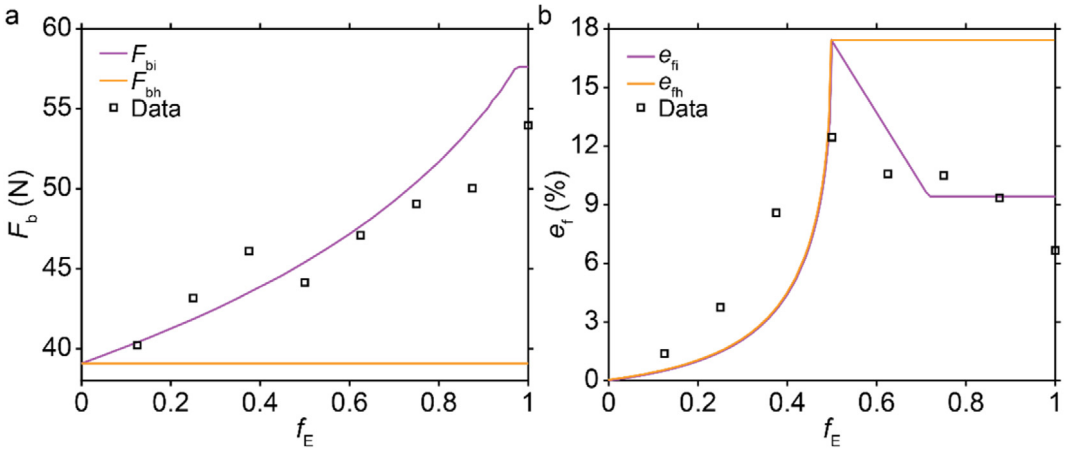

Fig. 6. Blocking force and free strain as a function of electrode coverage. (a) The measured values of the blocking force increase with the electrode coverage. The modeling results for inhomogeneous zipping (F_{bi}) agree well with the experimental data. For homogeneous zipping, the model predicts that the blocking force is independent of the electrode coverage (F_{bh}). (b) The measured values of the free strain increase with the electrode coverage until $f_E = 0.5$. In this range the model predicts for both types of zipping the same free strain, which qualitatively agrees with the experimental results. For $f_E > 0.5$, the measured values of the free strain decrease, because inhomogeneous zipping causes the bottom edge of the actuator to rotate. In this range of f_E, the model predicts no change in free strain for homogeneous zipping (e_{fh}). For inhomogeneous zipping (e_{fi}) the model predicts that the free strain initially decreases until it plateaus; while this trend seems to qualitatively agree with the experimental results, the underlying assumptions of the model are invalid at low loads (large strains) for values $f_E > 0.5$. (a)–(b) All actuators have the fill volume $V = 3.8$ ml. The experiments were performed at $\Phi = 6$ kV. (For interpretation of the references to color in this figure, the reader is referred to the web version of this article.).

Declaration of competing interest

N.K. and C.K. are listed as inventors on PCT application (PCT/US19/02056 8) and PCT application (PCT/US18/023797) which cover fundamentals and basic designs of HASEL actuators. P.R., N.K., and C.K. are listed as inventors on a U.S. provisional patent application (62/813,266) which covers composite and folding designs of HASEL actuators. N.K. and C.K. are co-founders of Artimus Robotics Inc., a start-up company commercializing HASEL actuators.

Acknowledgments

This work was supported by a National Science Foundation grant, USA grant for Cyber–Physical Systems (grant No. 1739452), a GAANN (Graduate Assistantships in Areas of National Need) Fellowship in Soft Materials, and a Packard Fellowship from The David and Lucile Packard Foundation, USA. We also acknowledge funding from the Army Research Office, United States (DURIP grant No. W911NF-18-1-0203), which was used to purchase laboratory equipment to characterize and fabricate actuators.

Appendix A. Supplementary data

Supplementary material related to this article can be found online at https://doi.org/10.1016/j.eml.2019.100542.

References

[1] S.M. Mirvakili, I.W. Hunter, Artificial muscles: Mechanisms, applications, and challenges, Adv. Mater. 30 (2018) 1704407, http://dx.doi.org/10.1002/adma.201704407.

[2] C. Laschi, B. Mazzolai, M. Cianchetti, Soft robotics: Technologies and systems pushing the boundaries of robot abilities, Sci. Robot. 1 (2016) 1–12, http://dx.doi.org/10.1126/scirobotics.aah3690.

[3] P. Polygerinos, N. Correll, S.A. Morin, B. Mosadegh, C.D. Onal, K. Petersen, M. Cianchetti, M.T. Tolley, R.F. Shepherd, Soft robotics: Review

of fluid-driven intrinsically soft devices; manufacturing, sensing, control, and applications in human-robot interaction, Adv. Eng. Mater. 19 (2017) 1700016, http://dx.doi.org/10.1002/adem.201700016.
[4] D. Rus, M.T. Tolley, Design, fabrication and control of soft robots, Nature 521 (2015) 467–475, http://dx.doi.org/10.1038/nature14543.
[5] P. Rothemund, A. Ainla, L. Belding, D.J. Preston, S. Kurihara, Z. Suo, G.M. Whitesides, A soft, bistable valve for autonomous control of soft actuators, Sci. Robot 3 (2018) eaar7986, http://dx.doi.org/10.1126/scirobotics.aar7986.
[6] A. Rafsanjani, Y. Zhang, B. Liu, S.M. Rubinstein, K. Bertoldi, Kirigami skins make a simple soft actuator crawl, Sci. Robot. 3 (2018) eaar7555, http://dx.doi.org/10.1126/scirobotics.aar7555.
[7] F. Ilievski, A.D. Mazzeo, R.F. Shepherd, X. Chen, G.M. Whitesides, Soft robotics for chemists, Angew. Chemie Int. Ed. 50 (2011) 1890–1895, http://dx.doi.org/10.1002/anie.201006464.
[8] D. Yang, B. Mosadegh, A. Ainla, B. Lee, F. Khashai, Z. Suo, K. Bertoldi, G.M. Whitesides, Buckling of elastomeric beams enables actuation of soft machines, Adv. Mater. 27 (2015) 6323–6327, http://dx.doi.org/10.1002/adma.201503188.
[9] R. Pelrine, High-speed electrically actuated elastomers with strain greater than 100%, Science 287 (2000) 836–839, http://dx.doi.org/10.1126/science.287.5454.836.
[10] Z. Suo, Theory of dielectric elastomers, Acta Mech. Solida Sin. 23 (2010) 549–578, http://dx.doi.org/10.1016/S0894-9166(11)60004-9.
[11] C. Keplinger, T. Li, R. Baumgartner, Z. Suo, S. Bauer, Harnessing snap-through instability in soft dielectrics to achieve giant voltage-triggered deformation, Soft Matter 8 (2012) 285–288, http://dx.doi.org/10.1039/C1SM06736B.
[12] M.D. Lima, N. Li, M. Jung de Andrade, S. Fang, J. Oh, G.M. Spinks, M.E. Kozlov, C.S. Haines, D. Suh, J. Foroughi, S.J. Kim, Y. Chen, T. Ware, M.K. Shin, L.D. Machado, A.F. Fonseca, J.D.W. Madden, W.E. Voit, D.S. Galvao, R.H. Baughman, Electrically, chemically, and photonically powered torsional and tensile actuation of hybrid carbon nanotube yarn muscles, Science 338 (2012) 928–932, http://dx.doi.org/10.1126/science.1226762.
[13] W.R.K. Illeperuma, J.-Y. Sun, Z. Suo, J.J. Vlassak, Force and stroke of a hydrogel actuator, Soft Matter 9 (2013) 8504, http://dx.doi.org/10.1039/c3sm51617b.
[14] M.M. Hamedi, V.E. Campbell, P. Rothemund, F. Güder, D.C. Christodouleas, J.-F. Bloch, G.M. Whitesides, Electrically activated paper actuators, Adv. Funct. Mater. 26 (2016) 2446–2453, http://dx.doi.org/10.1002/adfm.201505123.
[15] M. Shahinpoor, Y. Bar-Cohen, J.O. Simpson, J. Smith, Ionic polymer-metal composites (IPMCs) as biomimetic sensors, actuators and artificial muscles — a review, Smart Mater. Struct. 7 (1998) R15–R30, http://dx.doi.org/10.1088/0964-1726/7/6/001.
[16] R. Yoshida, T. Ueki, Evolution of self-oscillating polymer gels as autonomous polymer systems, NPG Asia Mater. 6 (2014) e107, http://dx.doi.org/10.1038/am.2014.32.
[17] W. Hu, G.Z. Lum, M. Mastrangeli, M. Sitti, Small-scale soft-bodied robot with multimodal locomotion, Nature 554 (2018) 81–85, http://dx.doi.org/10.1038/nature25443.
[18] M. Rogóz, H. Zeng, C. Xuan, D.S. Wiersma, P. Wasylczyk, Light-driven soft robot mimics caterpillar locomotion in natural scale, Adv. Opt. Mater. 4 (2016) 1689–1694, http://dx.doi.org/10.1002/adom.201600503.
[19] E. Acome, S.K. Mitchell, T.G. Morrissey, M.B. Emmett, C. Benjamin, M. King, M. Radakovitz, C. Keplinger, Hydraulically amplified self-healing electrostatic actuators with muscle-like performance, Science 359 (2018) 61–65, http://dx.doi.org/10.1126/science.aao6139.
[20] N. Kellaris, V. Gopaluni Venkata, G.M. Smith, S.K. Mitchell, C. Keplinger, Peano-hasel actuators: Muscle-mimetic, electrohydraulic transducers that linearly contract on activation, Sci. Robot. 3 (2018) eaar3276, http://dx.doi.org/10.1126/scirobotics.aar3276.
[21] S.K. Mitchell, X. Wang, E. Acome, T. Martin, K. Ly, N. Kellaris, V.G. Venkata, C. Keplinger, An easy-to-implement toolkit to create versatile and high-performance HASEL actuators for untethered soft robots, Adv. Sci. (2019) 1900178, http://dx.doi.org/10.1002/advs.201900178.
[22] N. Kellaris, V.G. Venkata, P. Rothemund, C. Keplinger, An analytical model for the design of Peano-HASEL actuators with drastically improved performance, Extreme Mech. Lett. 29 (2019) 100449, http://dx.doi.org/10.1016/j.eml.2019.100449.
[23] L. Maffli, S. Rosset, H.R. Shea, Zipping dielectric elastomer actuators: characterization, design and modeling, Smart Mater. Struct. 22 (2013) 104013, http://dx.doi.org/10.1088/0964-1726/22/10/104013.
[24] M. Righi, M. Fontana, R. Vertechy, M. Duranti, G. Moretti, Analysis of dielectric fluid transducers, in: Y. Bar-Cohen (Ed.), in: Electroact. Polym. Actuators Devices, vol. 10594, SPIE, 2018, p. 29, http://dx.doi.org/10.1117/12.2297082.
[25] R. Niiyama, X. Sun, C. Sung, B. An, D. Rus, S. Kim, Pouch motors: Printable soft actuators integrated with computational design, Soft Robot. 2 (2015) 59–70, http://dx.doi.org/10.1089/soro.2014.0023.
[26] J.-S. Plante, S. Dubowsky, Large-scale failure modes of dielectric elastomer actuators, Int. J. Solids Struct. 43 (2006) 7727–7751, http://dx.doi.org/10.1016/j.ijsolstr.2006.03.026.
[27] X. Zhao, W. Hong, Z. Suo, Electromechanical hysteresis and coexistent states in dielectric elastomers, Phys. Rev. B. 76 (2007) 134113, http://dx.doi.org/10.1103/PhysRevB.76.134113.
[28] A.N. Gent, Elastic instabilities in rubber, Int. J. Non. Linear. Mech. 40 (2005) 165–175, http://dx.doi.org/10.1016/j.ijnonlinmec.2004.05.006.
[29] J. Zhu, M. Kollosche, T. Lu, G. Kofod, Z. Suo, Two types of transitions to wrinkles in dielectric elastomers, Soft Matter 8 (2012) 8840, http://dx.doi.org/10.1039/c2sm26034d.
[30] T.-Q. Lu, Z.-G. Suo, Large conversion of energy in dielectric elastomers by electromechanical phase transition, Acta Mech. Sin. 28 (2012) 1106–1114, http://dx.doi.org/10.1007/s10409-012-0091-x.
[31] S.J.A. Koh, C. Keplinger, R. Kaltseis, C.-C. Foo, R. Baumgartner, S. Bauer, Z. Suo, High-performance electromechanical transduction using laterally-constrained dielectric elastomers part I: Actuation processes, J. Mech. Phys. Solids 105 (2017) 81–94, http://dx.doi.org/10.1016/j.jmps.2017.04.015.
[32] C. Keplinger, J.Y. Sun, C.C. Foo, P. Rothemund, G.M. Whitesides, Z. Suo, Stretchable, transparent, ionic conductors, Science 341 (2013) 984–987, http://dx.doi.org/10.1126/science.1240228.
[33] Y. Bai, B. Chen, F. Xiang, J. Zhou, H. Wang, Z. Suo, Transparent hydrogel with enhanced water retention capacity by introducing highly hydratable salt, Appl. Phys. Lett. 105 (2014) 151903, http://dx.doi.org/10.1063/1.4898189.